

Satellite and Radar Observations of the 9 April 2009 Texas and Oklahoma Grassfires

BY THOMAS A. JONES AND SUNDAR A. CHRISTOPHER

Dozens of large grassfires occurred throughout North Texas and southern Oklahoma on 9 April 2009, destroying hundreds of homes and businesses while burning thousands of acres of grasslands and causing millions of dollars in damages (Fig. 1a, *Times-Record News*—10 April 2009). Severe drought conditions existed throughout this region in the early part of 2009, according to the National Drought Mitigation Center (NDMC), resulting in large areas of dead, dry grass and brush that served as fuel for the ensuing fires. During the day, a dryline moved eastward through central Texas and southern Oklahoma, behind which strong westerly winds and very dry air were present over a large region. Strong winds picked up dry dust from western Texas, reducing visibility and air quality behind the dryline. Furthermore, these winds caused damage to power lines, sparking fires that spread very rapidly. Other fires were started by accident and/or produced by embers left over from previous grassfires that



FIG. 1. (a) Home and property destruction near Archer City, TX. (b) Steel-framed storage barn destroyed near Electra, TX. Note that the heat of the fire has deformed the metal frame. Photographs courtesy of the 10 Apr 2009 edition of the *Times-Record News* of Wichita Falls, TX.

AFFILIATIONS: JONES—Earth System Science Center, The University of Alabama in Huntsville, Huntsville, Alabama; CHRISTOPHER—Earth System Science Center, and Department of Atmospheric Science, The University of Alabama in Huntsville, Huntsville, Alabama

CORRESPONDING AUTHOR: Thomas A. Jones, Earth System Science Center, The University of Alabama in Huntsville, 320 Sparkman Drive, NSSTC, Huntsville, AL 35805
E-mail: tjones@nsstc.uah.edu

DOI:10.1175/2009BAMS2919.1

©2010 American Meteorological Society

had occurred during the prior week. The resulting fires persisted well into the evening hours of 9 April and were not completely under control until the next day. For example, intense heat from one fire deformed the steel frames of storage buildings, causing over \$20 million in damage to a single business in Electra,

TX (Fig. 1b). Several fires produced large smoke and debris plumes that were visible from various satellite and surface-based remote sensing platforms, such as the Moderate Resolution Imaging Spectroradiometer (MODIS) satellite-based sensor, as well as surface-based WSR-88D Doppler radars.

The catalyst for the 9 April fires was a deepening low-pressure system in northeastern Oklahoma associated with a dryline that became better defined as the afternoon progressed. Surface observations from Automated Surface Observing Systems (ASOS) stations reported dry ($RH < 20\%$), windy conditions behind the dryline. Westerly winds behind the dryline quickly increased to greater than 15 m s^{-1} , with a maximum gust of 34 m s^{-1} (or 76 mph) recorded southeast of Frederick, Oklahoma, at 1925 UTC. Winds remained strong throughout the afternoon and did not decrease substantially until well after 0000 UTC 10 April. Also of note are the low visibilities ($< 6 \text{ km}$) caused by the extreme amounts of dust in the atmosphere. In particular, visibility at both Abilene, Texas (KABI), and Dyess Air Force Base (KDYS) was often below 6 km between 1700 and 2200 UTC. Reduction in visibility due to smoke plumes was actually less than that observed for dust. Stations ahead of the smoke plumes included Gainesville, Texas (KGLE), and Ardmore, Oklahoma (KADM). Visibility at both locations decreased to around 8 km after 2200 UTC; however, lower visibilities likely existed nearer to the fires themselves. If not for the grassfires, the impacts of the dust storm would have been considered a significant event in itself.

Given the favorability of the environment for the propagation of grassfires over the region, it is not surprising that such a large outbreak occurred. These conditions were well-forecasted by the National Weather Service (NWS), who issued fire weather watches for the region 48 h in advance and a red flag warning early in the morning of 9 April. As the outbreak progressed, the Norman NWS Office (OUN) issued multiple nowcasts and fire-warning products stating the locations and predicted near-term evolution of individual fires using data from various surface and remote-sensing data sources. The number of fires was such that warnings were being issued similar to the frequency typically seen during large severe-weather outbreaks. However, during the latter, more automated tools exist to examine the incoming raw data directing where the forecaster should focus their resources. These tools do not yet exist for short-term fire forecasts, and part

of this ongoing research is to assess how data from remote-sensing platforms such as satellite and radars can be used in the creation of such tools.

The MODIS instrument on the *Terra* and *Aqua* satellites measures reflected and emitted radiation from the Earth-atmosphere system in the ultraviolet (UV) to the thermal infrared (IR). Visible reflectance and brightness temperature data at 1-km resolution can be used to determine the locations and spatial extent of dust and smoke present in the atmosphere. For illustration purposes, the MOD14 MODIS fire-detection product was obtained for the same time period. Fires are identified using a contextual algorithm for fire detection that report the location and temperatures of various “hotspots” at the time of the satellite overpass. A false color image of *Aqua* MODIS data at approximately 1930 UTC (or 2:30 p.m. local time) clearly shows the location of the individual fires and the downwind smoke plumes, as well as the large dust storm also present over the region (Fig. 2). Smoke plumes existed more than 100 km downwind of the strongest fires, whose approximate origin is given by the MODIS (MOD14 product) hotspot detections within Fig. 2. The greatest concentration of hotspots was located in south central Oklahoma and North Texas. Other important features include a north-to-south-oriented line of clouds located east of and along the dryline. Another line of clouds is present in western Oklahoma associated with a cold front moving southeastward behind the dryline. The maximum intensity of the fires occurred in this window after the passage of the dryline, but before the passage of the cold front, behind which winds were somewhat weaker.

Spectral signatures from multiple reflectance and brightness temperature channels are often used to separate various features within satellite imagery, such as dust and smoke aerosols from clouds and the underlying background. Aerosols such as dust and especially smoke generally reflect more visible radiation back into space than darker backgrounds such as water or vegetated surfaces, making smoke and dust plumes appear brighter in a satellite image. The darker the background, the easier aerosols can be observed. Smoke aerosols have submicron particle sizes and are primarily sensitive to wavelengths less than $1.0 \mu\text{m}$. At longer wavelengths, smoke aerosols do not reflect incoming solar radiation and the satellite simply senses the underlying surface. Dust plumes have larger particle sizes with effective radii between 1.0 and $2.0 \mu\text{m}$ compared to submicron smoke aerosols, and the

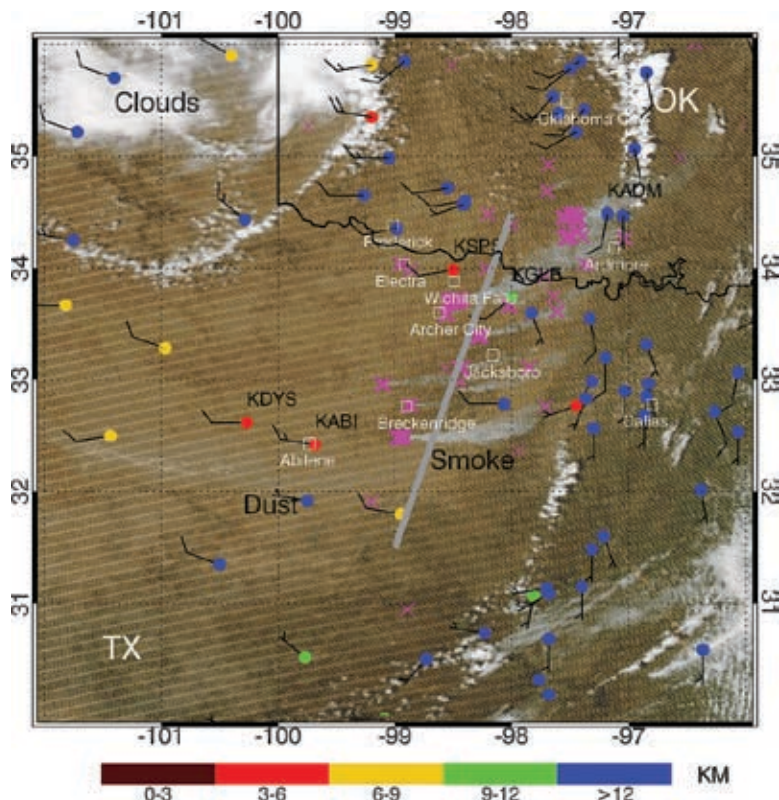


FIG. 2. Aqua MODIS level IB false-color image of North Texas and southern Oklahoma at 1930 UTC 9 Apr 2009 created using 0.47-, 0.55-, and 0.67- μm visible reflectance. Individual smoke plumes are clearly evident as grayish-white regions aligned in a north-to-south manner between southern Oklahoma and North Texas, with individual smoke plumes extending eastward. MODIS hotspots at this time are denoted as pink X's and show the location of the individual fires. ASOS surface stations are also plotted and color-coded to represent visibility at each site, with blue indicating > 12 km visibility and red indicating < 6 km visibility. Wind speed and direction are given by wind barbs at each station with long flags corresponding to 10 m s^{-1} and short flags being 5 m s^{-1} . Southwest-northeast oriented gray line represents the line through which cross sections of satellite and radar data were examined and shown in Fig. 3. X- and Y-axis values represent degrees of longitude and latitude, respectively.

brightness temperature difference between 11- and 12- μm infrared bands is often used to separate dust from the background regions and/or clouds.

To compare the spectral signature of dust relative to smoke, a cross section of MODIS visible reflectance and infrared brightness temperature data was analyzed from 31.5° to 34.5°N (Fig. 3a). This cross section passes through two of the largest smoke plumes (32.5° and 33.7°N, labeled as F1 and F2, respectively) as well as several smaller ones in between (Figs. 2 and 4). Visible reflectance (0.67 μm) showed a distinct increase near the location of the smoke plumes, since they were

brighter than the surface background. Along this cross section, no significant cloud cover was present; thus, changes in visible reflectance were almost certainly due to aerosols. The dust storm was also evident between 31.5° and 33.0°N, where the brightness-temperature difference between 11- and 12- μm MODIS data is negative. However, this difference also became negative in the vicinity of the smoke plume from F2. Visibilities remained high in the area surrounding F2; thus, widespread dust was likely not the reason for this signal. The cause of this signal was likely due to the larger debris being lofted into the atmosphere, especially since the difference quickly returns to near-zero away from the smoke plume associated with F2. For F1, the increase in 0.67- μm reflectance relative to the surrounding dust is the key indicator of the location of the smoke within the larger dust plume, though debris within the smoke plume itself can give a spectral signal similar to that of dust.

Further quantitative assessment of the 2D and even 3D characteristics of smoke plumes can be inferred from WSR-88D radar observations. The WSR-88D is an active S-Band (10 cm) Doppler precipitation radar, with an azimuthal resolution of 1° and a range bin of 1 km providing a 3D data volume every 5 to 6 minutes. The 9 April fires occurred within range of four WSR-88Ds (KTLX, KFDR, KDYS, and KFWS, located near Oklahoma City and Frederick, Oklahoma, and

Abilene and Dallas, Texas, respectively), providing excellent spatial sampling over a large area. It is important to note that these radars are not sensitive to the smoke or aerosols themselves that have particle diameters (D) less than one micron, but the much larger burnt grass and other debris ($D > 100 \mu\text{m}$) lofted into the atmosphere by the buoyant updrafts associated with the stronger fires. Both radar and satellite sensors can sample various characteristics of the fires and resulting smoke plumes, and a combination of these data can provide a greater understanding of grassfire properties and evolution previously not possible.

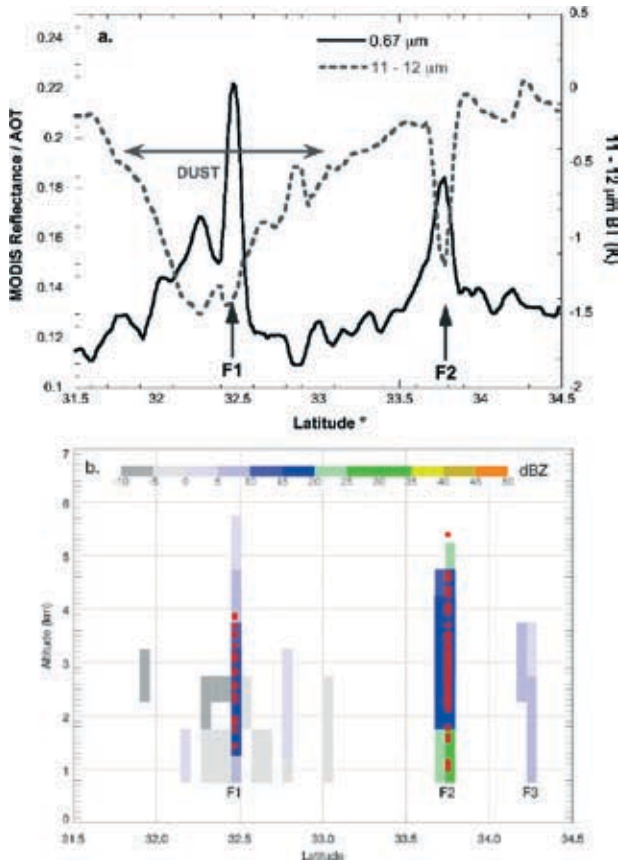


FIG. 3. (a) Cross section of MODIS 0.67- μm reflectance and 11–12- μm brightness temperature between 31° and 34.5°N at 1930 UTC corresponding to the gray line in Fig. 2 showing the location of the dust and smoke plumes emanating from fires F1 and F2. See Fig. 4 for geographical locations of F1–F4 relative to the cross-section line. (b) Cross section of radar reflectivity data at 1945 UTC from KDYX, KFDR, KFWS, and KTLX between 31° and 34.5°N, with locations of F1, F2, and F3 denoted (b). Algorithm-estimated debris heights corresponding to F1 and F2 within ± 30 minutes of the radar time are also shown.

To objectively estimate debris height from WSR-88D data, we use a modified version of the Storm Cell Identification and Tracking (SCIT) algorithm, which was designed to detect and report spatial and temporal characteristics of individual storm cells. The maximum height parameter, or storm top, defines the highest level at which reflectivity greater than a predefined threshold exists. For this research, the storm-top parameter represents an estimate of the maximum height to which debris-sized particles are being transported. Data associated with actual precipitation features were removed manually, but in the future it will be possible to use WSR-88Ds upgraded

with dual-polarimetric capabilities to distinguish between precipitation and biomass debris. Debris lofted into the air from fires is generally nonspherical in nature and has much different scattering properties than raindrops, thereby allowing for a clear distinction between the two.

While the radars are not sensitive to the smoke-sized particles themselves, they are sensitive to the large burnt debris lofted into the atmosphere by the fire and transported downstream by the prevailing winds. Since the smoke aerosols are submicron in size, it can be surmised that if debris is being detected by the radar, then large concentrations of smoke aerosols should be also be present. Dust aerosols are not associated with debris plumes and as a result are not readily detectable from precipitation radars. Thus, in a complex environment that includes a dust storm and a grassfire outbreak, radars can be quickly used to distinguish one from the other.

The locations of several fires are evident using WSR-88D reflectivity data (dBZ) combined from KDYX, KFDR, KFWS, and KTLX radars over a domain roughly 350 by 350 km² at 1945 UTC (Fig. 4). The four strongest fires at 1945 UTC are labeled as F1 through F4 (Fig. 4), with their origin being near Breckenridge (F1), Archer City (F2), and Electra, Texas (F3), and southwest of Ardmore, Oklahoma (F4). Debris plumes from each fire extend east-northeast and are visible up to 100 km away from the source fire. At this time, the plume associated with F2 is the strongest, producing reflectivity values in excess of 25 dBZ. If this were precipitation, this reflectivity would correspond to light rainfall. The debris from F2 becomes mixed in with the debris produced by F4 in southern Oklahoma and extending into central Oklahoma. Substantial debris plumes are also evident with F1 and F3, with several smaller plumes present throughout North Texas. Nearly all the radar reflectivity associated with the fires exists behind the dryline, which can be seen as a thin line of reflectivity extending between KFWS and KTLX.

Given the relatively large size of the debris ($D > 100 \mu\text{m}$), it would generally be expected to fall out of the atmosphere within an hour or less, limiting its potential to be transported far downstream. In this case, winds gusting to 30 m s^{-1} easily allow a downstream transport of 100 km or more before some radar-observable particles would finally fall out of the atmosphere, which is consistent with the radar observations. However, not all the debris travels this distance, as at least some of the further

downstream debris likely originates from the fires seeded by the original debris plume. Further north, the debris plumes associated with F3 and F4 were generally smaller and shorter lived. Fire F3, which destroyed homes and businesses in Electra (Fig. 1b), was visible as a long, thin debris plume at 1945 UTC, but weakened quickly and was no longer visible after 2100 UTC. Fire F4 in southern Oklahoma was composed of several small fires in close proximity to one another combining to produce a large single debris plume, but reflectivity was not as great as in the other plumes, indicating smaller amounts of large debris being injected high into the atmosphere.

The debris plume observations from radar agree well with satellite-based smoke plume observations, indicating that both are collocated in space and time. Using this assumption, radar data can be used to estimate the height to which debris (and, by extrapolation, smoke aerosols) is lofted into the atmosphere. A cross section of radar data through the stronger smoke plumes indicates the grass and other burnt debris are reaching at least 5 km into the atmosphere (Fig. 3b). Maximum reflectivity values are again associated with F2, with reflectivity greater than 20 dBZ being observed at 5 km. To transport the debris necessary for reflectivity values at this height, the heat-induced updrafts corresponding to the fire must be quite intense. The locations of the debris plumes based on radar data correspond almost exactly to the locations of low MODIS visible reflectance values calculated along the same path, with one exception (Fig. 3). Weak reflectivity corresponding to F3 is visible near 34.3°N, but the overall smoke plume associated with F3 has dispersed to the extent that it is not visible in the satellite cross section (Fig. 3a).

Plume heights generated from modified severe-storm algorithms provide a unique insight into the evolution of individual fires in terms of intensity and the height to which debris is being lofted into the atmosphere. This is made possible by the similarity of the size and shape of individual debris plumes to supercell thunderstorms; thus, the severe-weather algorithms can be tricked into returning characteristics of these “storms,” which can be used for additional analysis. Algorithm detection of the debris plumes primarily occurred within a 6-h window between 1800 and 0000 UTC, with all major debris plumes being detected at one point or another. Detections associated with the major fires within ± 30 minutes of 1945 UTC are shown in Fig. 4 along with the raw radar data. These same detections for F1 and F2 are also plotted on the radar

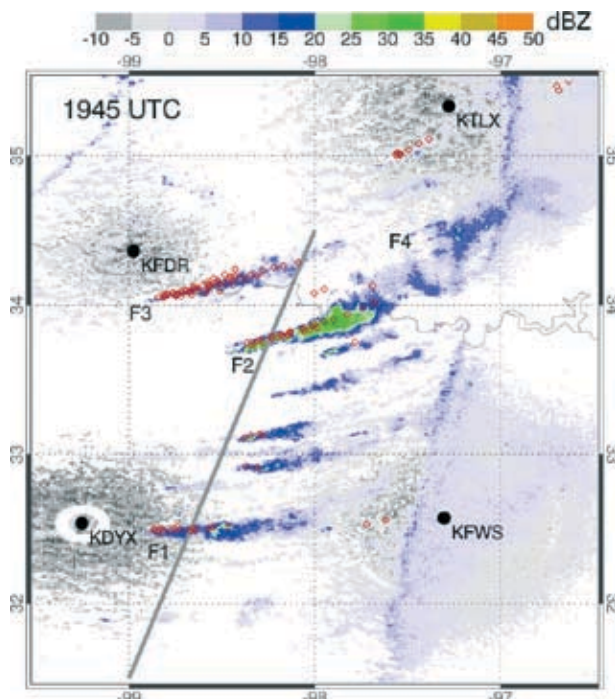


FIG. 4. WSR-88D radar reflectivity data (dBZ) from KDYX, KFDR, KFWS, and KTLX at 1945 UTC 9 Apr. Approximate height of radar data is 1 km, with a spatial resolution of 1 km. Many fires are clearly evident, with some having debris plumes greater than 100 km in length. Overlaid as red dots are SCIT “storm cell” detections for each debris plume within ± 30 minutes of this time. As in Fig. 2, the cross-section line is plotted in gray. Four individual fires are denoted (F1, F2, F3, and F4), each representing the origin of large radar-detectable debris plumes. X- and Y-axis values represent degrees of longitude and latitude, respectively.

cross section in Fig. 3b and correspond to the locations of both the enhanced values of reflectivity as well as the increased satellite reflectance. The greatest number of algorithm-estimated debris heights occurs between 2 and 4 km for F1 and F2, indicating that the debris and smoke are reaching well above the boundary layer of the atmosphere.

Using both satellite and ground-based remote-sensing platforms, we are able to assess the 9 April 2009 grassfires in great detail. Multispectral observations from the MODIS data proved useful in detecting the locations of both dust and smoke. Precipitation radars were unable to sample aerosols associated with the dust storm, but did sample debris associated with the individual fires in both high spatial and temporal resolutions. The location of individual debris plumes from radar corresponded well with available satellite obser-

vations in both initiation location and spatial extent of downstream smoke plumes. Radar data were also useful at determining the height to which debris was being injected into the atmosphere, which was greater than 5 km for the strongest fires. Smoke and debris lofted this high can remain in the atmosphere for hours and during this event affect conditions over 100 km downwind of the fires themselves. Currently, no objective system exists that uses all these data sources in near-term fire weather and/or air quality forecasts. Given the detailed observations of the 9 April fire made possible by these data, we believe inclusion of such data will be extremely advantageous in future fire weather forecasting. This will lead to improvements in various fire-related impacts, such as downstream air quality and emergency management (i.e., disbursement of fire-fighting resources and where future evacuations are necessary).

ACKNOWLEDGMENTS. This work is supported by NOAA Air Quality grants at UAHuntsville. The MODIS data were acquired through the Level 1 and Atmosphere Archive and Distribution System, and GOES ABBA data from the NRL FLAMBE project. WSR-88D Level 2 radar data were acquired from the NCDC archive using the HDSS Access System.

FOR FURTHER READING

- Banta, R. M., L. D. Olivier, E. T. Holloway, R. A. Kropfli, B. W. Bartram, R. E. Cupp, and M. J. Post, 1992: Smoke-column observations from two forest fires using Doppler lidar and Doppler radar. *J. Appl. Meteor.*, **31**, 1328–1349.
- Crum, T. D., and R. L. Alberty, 1993: The WSR-88D and the WSR-88D Operational Support Facility. *Bull. Amer. Meteor. Soc.*, **74**, 1669–1687.
- Johnson, J. T., P. L. MacKeen, A. Witt, D. Mitchell, G. J. Stumpf, M. D. Eilts, and K. W. Thomas, 1998: The Storm Cell Identification and Tracking algorithm: An enhanced WSR-88D algorithm. *Wea. Forecasting*, **13**, 263–276.
- Jones, T. A., and S. A. Christopher, 2009: Injection heights of biomass burning debris estimated from WSR-88D radar observations. *IEEE Trans. Geosci. Remote Sens.*, **47**, 2599–2605.
- Jones, T. A., S. A. Christopher, and W. Petersen, 2009: Dual polarimetric radar characteristics of an apartment fire. *J. Oceanic Atmos. Technol.*, in press.
- Justice, C. O., and Coauthors, 2002: The MODIS fire products. *Remote Sens. Environ.*, **83**, 244–262
- Melnikov, V. M., D. S. Zurnic, and R. M. Rabin, 2008: Radar polarimetric signatures of fire plumes in Oklahoma. *Geophys. Res. Lett.*, **35**, L14815, doi:10.1029/2008GL034311.
- National Weather Service, Norman Oklahoma, cited 2009: Event summary for the wildfire outbreak of April 9, 2009. [Available online at: www.srh.noaa.gov/oun/?n=events-20090409.]
- Prospero, J. M., P. Ginoux, O. Torres, and S. Nicholson, 2002: Environmental characterization of global sources of atmospheric soil dust derived from NIMBUS-7 TOMS absorbing aerosol product. *Rev. Geophys.*, **40**, 1002, doi:10.1029/2000RG000095.
- Rothermel R. C., 1991: Predicting behavior and size of crown fires in the northern Rocky Mountains. Res. Pap. INT-438. U. S. Dept. of Agriculture, 46 pp.
- Sokolik, I., and O. Toon, 1999: Incorporation of mineralogical composition into models of the radiative properties of mineral aerosol from UV to IR wavelengths. *J. Geophys. Res.*, **104** (D8), 9423–9444.
- Wilhite, D. A., K. H. Smith, and M. J. Hayes, 1996: The National Drought Mitigation Center. *Proc. Conserv '96*, American Water Works Association, 795–799.